Excited-state quantum phase transitions in Dicke superradiance models

Tobias Brandes
Institut für Theoretische Physik, Technische Universität Berlin, Hardenbergstraße 36, D-10623 Berlin, Germany
(Received 1 July 2013; published 23 September 2013)

We derive analytical results for various quantities related to the excited-state quantum phase transitions in a class of Dicke superradiance models in the semiclassical limit. Based on a calculation of a partition sum restricted to Dicke states, we discuss the singular behavior of the derivative of the density of states and find observables such as the mean (atomic) inversion and the boson (photon) number and its fluctuations at arbitrary energies. Criticality depends on energy and a parameter that quantifies the relative weight of rotating versus counterrotating terms, and we find a close analogy to the logarithmic and jump-type nonanalyticities known from the Lipkin-Meshkov-Glick model.

DOI: 10.1103/PhysRevE.88.032133 PACS number(s): 05.30.Rt, 42.50.Nn, 64.70.Tg

I. INTRODUCTION

The recent successful experimental realization [1] of the Dicke-Hepp-Lieb superradiance [2,3] with cold atoms in photonic cavities has sparked a renewed interest in the Dicke model. Although a detailed understanding of the quantum phase transition (QPT) associated with the phenomenon requires somewhat more involved modeling [4–8], the simplest one-mode form of the Dicke Hamiltonian (a boson coupled to a large angular momentum) continues to serve as a simple model with fascinating properties. One reason for this is the nonintegrability of the model and the appearance of quantum chaos and its relation to the bifurcation-type QPT in the thermodynamic limit $N \to \infty$ of infinitely many (pseudo-spin $\frac{1}{2}$) two-level systems [9–12].

Apart from various modifications of the model for adaptation to, e.g., multilevel systems [13,14] or realizations in other materials [15–17], the Dicke model has been discussed recently [18–20] in the context of excited-state quantum phase transitions (ESQPTs). In contrast to ground-state QPTs, these occur at higher energies and have singularities in the energy level structure as their hallmark [21,22]. Numerical calculations [18] confirmed a line of ESQPTs in the superradiant phase of the Dicke model at the energy coinciding with the ground-state energy of the normal phase. In a semiclassical picture, this energy corresponds to the excitation energy from a spontaneously symmetry-broken ground state right onto the top of a local maximum in a Landau functional-type potential.

Most of the research on ESQPTs so far has been dealing with mean-field-type Hamiltonians, where a classical potential landscape governs the singularities for both types of quantum phase transitions (see [18] for further references). This is also the case for the Lipkin-Meshkov-Glick (LMG) model [23] that describes a simple nonlinearity for a large angular momentum and for which Ribeiro, Vidal, and Mosseri [24,25] presented an exhaustive analysis of the phase diagram. Our results for the class of Dicke superradiance models discussed in this paper reveal a very close analogy to their findings for the LMG model, but they also show interesting aspects that are particular to the superradiance case and highlight the role of the semiclassical limits $N \to \infty$ and $\hbar \to 0$ at constant $N\hbar$ [11,12] for the level density $\nu(E)$ and all quantities derived from it.

In our model we introduce a control parameter g that quantifies the relative weight of rotating versus counterrotating terms [26,27], which corresponds to the amount of anisotropy in the LMG model coupling parameters. As a limit of particular interest we then obtain the Tavis-Cummings model [28], where the integrability leads to a Goldstone mode that persists throughout the superradiant phase and removes a logarithmic ESQPT singularity in favor of a first-order jump-type discontinuity, with a reemergence of the former if the Hilbert space is properly restricted to a single-excitation number only.

The key difference between ESQPT and finite-temperature phase transitions in quantum systems is the role of entropy. The ESQPT in the Dicke model appears in the Hilbert space spanned by the Dicke states $|jm\rangle$ with fixed $j = N/2$. The level density [density of states (DOS)] $\nu(E)$ of the eigenstates of the Hamiltonian of energy E then defines a microcanonical ensemble that is abnormal in the thermodynamic sense that the associated entropy $S(E) \equiv \ln \nu(E)$ does not scale linearly with the particle number N, but only logarithmically, i.e., $\nu(E)$ itself is only proportional to N. In contrast, the canonical partition sum $Z(T)$ that determines the original calculations [29,30] for finite-temperature phase-diagram sums over all 2^N states of the two-level systems. The saddle point approximation to $Z(T)$ for $N \to \infty$ contains the typical entropic contribution reflecting the high degree of degeneracy in that case and thermodynamic quantities such as free energy and entropy are extensive, i.e., proportional to N.

The structure of this paper is a follows. Section II describes the model and the main method, Sec. III discusses some general properties of the level density $\nu(E)$, and Sec. IV is devoted to a detailed discussion of the Dicke model. In Sec. V we then describe the ESQPTs in the generalized Dicke models, in Sec. VI we discuss the somewhat exceptional case of the restricted Tavis-Cummings model, and we conclude in Sec. VII. Appendixes A–D give some technical details on the angular momentum traces, the integrations needed in the Dicke model, the logarithmic singularities, and the Bogoliubov transformation for the normal phase of the generalized Dicke models.

II. MODEL AND METHOD

A. Hamiltonian

Our model describes a single bosonic cavity mode $a^\dagger$ coupled to N two-level systems that are described by a

collective angular momentum algebra $J_\alpha \equiv \frac{1}{2}\sum_{j=1}^{N}\hat{\sigma}_\alpha^{(j)}$, where $\alpha = x,y,z$ with $J_\pm \equiv J_x \pm i J_y$ and Pauli matrices $\hat{\sigma}_\alpha^{(j)}$. The Hamiltonian reads

$$\mathcal{H} = \hbar\omega a^\dagger a + \hbar\omega_0 J_z + \frac{\hbar\lambda}{\sqrt{N}}\sum_\pm \frac{1\pm g}{2}(aJ_\pm + a^\dagger J_\mp), \quad (1)$$

where $0 \leqslant g \leqslant 1$ is a parameter weighting rotating and counterrotating terms such that for $g = 0$, $\mathcal{H}$ describes the nonintegrable Dicke model (rotating and counterrotating terms), whereas $g = 1$ describes the integrable Tavis-Cummings model (rotating terms only). The model has a ground-state QPT when the criticality parameter

$$\mu \equiv \frac{\lambda^2}{\omega\omega_0} \quad (2)$$

equals unity, with the transition from the normal phase ($\mu < 1$) to the superradiant phase $\mu > 1$. Importantly, for our choice of coupling [31] the ground-state QPT and all ground-state quantities are independent of the value of g [26], whereas g will turn out as a control parameter for the ESQPT in the superradiant phase.

In the particular case $g = 1$ (Tavis-Cummings model), the Hamiltonian $\mathcal{H}$ conserves the excitation number

$$N_{\rm ex} \equiv a^\dagger a + J_z + j, \quad (3)$$

where again $j = N/2$ and one has to specify the value(s) of $N_{\rm ex}$ for which the QPT is discussed. In contrast, the $g \neq 1$ case only conserves a parity defined by $(-1)^{N_{\rm ex}}$.

We will include the limit $g = 1$ in the discussion for $0 \leqslant g < 1$ below in a natural way by defining an unrestricted Tavis-Cummings model where the calculation is performed by averaging over all values of $N_{\rm ex}$. In the last section, we then return to the Tavis-Cummings model restricted by a fixed excitation number, which turns out to be technically somewhat more involved than the unrestricted case. If fact, QPT criticality is (for our choice of coupling strengths) determined by the condition $\lambda > |\omega_0 - \omega|/2$ in that case regardless of $N_{\rm ex}$ [18].

B. Partition sum

The key quantity to obtain the level density (DOS) $\nu(E)$ is the partition sum $\mathcal{Z}(\beta)$,

$$\mathcal{Z}(\beta) \equiv {\rm Tr} e^{-\beta\mathcal{H}} \equiv \int_{E_0}^{\infty} dE\, e^{-\beta E}\nu(E), \quad (4)$$

from which $\nu(E)$ follows via Laplace back-transformation. Here E_0 is the ground-state energy of $\mathcal{H}$ [32].

We evaluate $\mathcal{Z}(\beta)$ by the method of Wang and Hioe [29] using coherent photon states and the limit $N \to \infty$ (which we will always consider in the following), whereby the operators $a, a^\dagger$ can be replaced by numbers α, α^* and one obtains

$$\begin{aligned}\mathcal{Z}(\beta) &= \int \frac{d^2\alpha}{\pi} e^{-\beta\hbar\omega|\alpha|^2} Z(\alpha;\beta),\\ Z(\alpha;\beta) &\equiv {\rm Tr}\left[-\beta\hbar\left(\omega_0 J_z + \frac{\lambda}{\sqrt{N}}\sum_\pm \frac{1\pm g}{2}(\alpha J_\pm + \alpha^* J_\mp)\right)\right].\end{aligned} \quad (5)$$

The next step is to evaluate the angular momentum trace $Z(\alpha;\beta)$ (which is taken over the basis of Dicke states $|jm\rangle$ with maximum $j = N/2$ only [33]) by employing the semiclassical limit $\beta\hbar\omega_0 \to 0$. In the energy domain, this means that we are interested in energies E that are macroscopic with respect to $\hbar\omega_0$ in the sense that the scaled energy

$$\varepsilon \equiv \frac{E}{N\hbar\omega_0} \quad (6)$$

is of order one. The semiclassical limit is thus formally defined as $\hbar \to 0$ together with the thermodynamic limit $N \to \infty$ such that the product $L \equiv \hbar j = \hbar N/2$ remains finite, where L is the conserved classical angular momentum [12]. The evaluation of $Z(\alpha;\beta)$ (Appendix A) yields

$$\mathcal{Z}(\beta) = \int_1^\infty dy \int_0^{2\pi} d\varphi \frac{N\sum_\pm \pm e^{N\beta\hbar\omega_0\Phi_\pm(\alpha(\varphi),y)}}{4\pi\mu\beta\hbar\omega g}, \quad (7)$$

where we defined the two dimensionless functions

$$\Phi_\pm(\alpha,y) \equiv -\frac{\alpha}{4}(y^2-1) \pm \frac{y}{2} \quad (8)$$

that play an important role in the following analysis and the φ-dependent function

$$\alpha(\varphi) \equiv \frac{1}{\mu}\left(1 + \frac{1-g^2}{g^2}\sin^2\varphi\right). \quad (9)$$

C. Density of states

The density of states $\nu(E)$ is determined by the inverse Laplace transformation

$$\mathcal{L}^{-1}\left[\frac{e^{N\beta\hbar\omega_0\Phi_\pm}}{\beta}\right](E) = \theta(E + N\hbar\omega_0\Phi_\pm) \quad (10)$$

under the integrals in Eq. (7), from which we obtain our first key expression

$$\begin{aligned}\nu(\varepsilon) &= \frac{N}{\hbar\omega}\int_0^{2\pi}\frac{d\varphi}{4\pi\mu g} I(\varphi),\\ I(\varphi) &\equiv \sum_\pm \pm \int_1^\infty dy\, \theta(\varepsilon + \Phi_\pm(\alpha(\varphi),y)),\end{aligned} \quad (11)$$

with the unit step function $\theta(x)$. We thus find $\nu(\varepsilon)$ as a product of the system size $N = 2j$, the constant DOS $1/\hbar\omega$ (corresponding to the semiclassical limit $\beta\hbar\omega \to 0$ of a single-oscillator mode with frequency ω), and a term that only depends on the dimensionless energy ε [Eq. (6)] and the parameters μ [Eq. (2)] and g.

III. LIMITING CASES OF $\nu(\varepsilon)$

The physics contained in the level density $\nu(\varepsilon)$ is quite rich and it is therefore instructive to consider limiting cases before analyzing the full analytical expressions to be derived from Eq. (11).

A. Noninteracting case

Already the noninteracting case $\lambda = 0$ shows some general features of $\nu(E)$ that persist in the interacting case too. We directly obtain the DOS by the inverse Laplace transformation

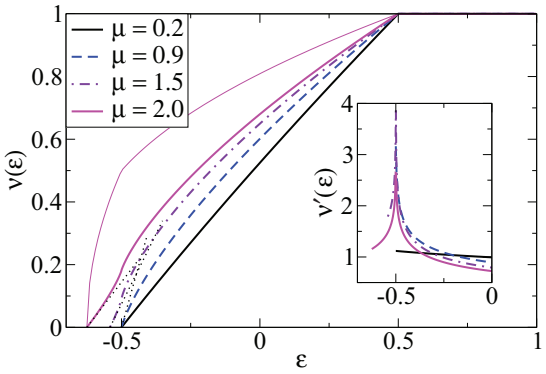

FIG. 1. (Color online) The DOS $\nu(\epsilon)$ (in units $N/\hbar\omega$) as a function of scaled energy $\varepsilon \equiv E/N\hbar\omega_0$ for the Dicke model ($g = 0$) at different values of criticality parameters $\mu \equiv \lambda^2/\omega\omega_0$. The thin solid line indicates the DOS $\nu(\epsilon)$ for the unrestricted Tavis-Cummings model (17) at $\mu = 2$ and the dotted lines indicate the slopes that are determined by the product of the collective excitation energies $\epsilon_\pm$ near the lower band edge (24). The inset shows the DOS derivative $\nu'(\varepsilon)$ (in units $N/\hbar^2\omega\omega_0$) displaying the logarithmic ESQPT singularity at $\varepsilon = -\frac{1}{2}$ for $\mu > 1$.

of Eq. (5) or via $\nu(E) = \sum_{n=0}^{\infty}\sum_m \delta(E - \hbar\omega n - \hbar\omega_0 m)$ again using the limits $N \to \infty$ and $\hbar \to 0$, thus converting sums into integrals,

$$\nu(\varepsilon) = \frac{N}{\hbar\omega}\begin{cases} 0, & \varepsilon \leqslant -\frac{1}{2} \\ \frac{1}{2} + \varepsilon, & |\varepsilon| < \frac{1}{2} \\ 1, & \varepsilon \geqslant \frac{1}{2}, \end{cases} \tag{12}$$

where $\varepsilon = -\frac{1}{2}$ is the scaled ground-state energy for $\lambda = 0$ (no bosons, all lower atomic levels occupied). Above this lower band edge, $\nu(E)$ grows linearly with a slope $(\hbar^2\omega\omega_0)^{-1}$, followed by a constant DOS $N/\hbar\omega$ when $E > N\hbar\omega_0/2$, the total energy of the upper atomic levels. Graphically, $\nu(\varepsilon)$ is very close to the weak-coupling ($\mu = 0.2$) curve in Fig. 1.

The simple form (12) of $\nu(\varepsilon)$ also follows from the convolution $\nu(E) = \int_{-\infty}^{\infty} dE' \nu_{\rm osc}(E - E')\nu_{\rm ang}(E')$ with the boson and angular momentum DOS $\nu_{\rm bos}(E) = \theta(E)/\hbar\omega$ and $\nu_{\rm ang}(E) = \theta(\hbar\omega_0/2 - |E/N|)/\hbar\omega_0$ in the semiclassical limit.

B. Band edges

As a matter of fact, even for arbitrary g and μ one has

$$\nu(\varepsilon) = \frac{N}{\hbar\omega}, \quad \varepsilon \geqslant \frac{1}{2}. \tag{13}$$

To prove Eq. (13), we note that the argument of the step function in Eq. (11) is a downward parabola as a function of y with zeros

$$y^\sigma_{1,2} \equiv \frac{\sigma}{\alpha(\varphi)} \mp \sqrt{\frac{1}{\alpha(\varphi)^2} + 1 + \frac{4\varepsilon}{\alpha(\varphi)}}, \quad \sigma = \pm, \tag{14}$$

where the index 1 (2) belongs to the negative (positive) root. For energies below $\varepsilon = \frac{1}{2}$, we have $y_1^- < y_2^- < 1$ and only the plus part in the sum $\sum_\pm$ contributes to $\nu(\varepsilon)$ in Eq. (11). In contrast, for energies above $\varepsilon = \frac{1}{2}$, we find $y_1^+ < -1$, $y_2^+ > 1$, $y_1^- < -1$, and $y_2^- > 1$ and the y integral is given by $I(\varphi) = \sum_\pm \pm(y_2^\pm - 1) = 2/\alpha(\varphi)$. For the remaining φ integration we now use

$$\int_0^\pi d\varphi \frac{1}{a - b\sin^2\varphi} = \frac{\pi}{\sqrt{a}\sqrt{a-b}} \tag{15}$$

to find Eq. (13) at arbitrary g and μ.

The energy $\varepsilon = \frac{1}{2}$ thus plays the role of an upper edge for nontrivial behavior of the DOS $\nu(\varepsilon)$. For $\varepsilon > 1/2$, $\nu'(\varepsilon)$ vanishes and the DOS is solely determined by the oscillator frequency ω. In particular, in this high-energy limit $\nu(\varepsilon)$ does not depend on the two-level energy $\hbar\omega_0$. Note that the nonanalyticity of $\nu(\varepsilon)$ at $\varepsilon = \frac{1}{2}$ resulting from Eq. (13) is not an ESQPT, as it is not related to the interaction between the boson and the two-level systems: It also occurs for $\lambda = 0$, where it reflects the disparity between the unbounded boson and the bounded angular momentum DOS.

The lower band edge, in contrast, is determined by the ground-state energy, which is given by $E = -N\hbar\omega_0/2$ ($\varepsilon = -\frac{1}{2}$) in the normal phase and

$$\varepsilon_0 \equiv \frac{E_0}{N\hbar\omega_0} \equiv -\frac{1}{4}\left(\mu + \frac{1}{\mu}\right) \tag{16}$$

in the superradiant phase. This (known) result for E_0 also follows from the asymptotic behavior of the partition sum $\mathcal{Z}(\beta)$ for $\beta \to \infty$. The interval $[\varepsilon_0, \frac{1}{2}]$, which we will call the band for the rest of the paper, therefore defines the region of nontrivial excited-state physics for the $N \to \infty$ limit of our model.

C. Unrestricted Tavis-Cummings model

For $g = 1$, the φ integration in Eq. (11) is trivial and the result for $\nu(\varepsilon)$ is determined by the boundaries of the y integral due to the step function, which can be expressed in terms of the zeros (14). As a result, we find $\nu(\varepsilon) = N(y_2^+ - y_1^+)/2\hbar\omega\mu$ for $\varepsilon_0 \leqslant \varepsilon \leqslant -1/2$, $\nu(\varepsilon) = N(y_2^+ - 1)/2\hbar\omega\mu$ for $-1/2 \leqslant \varepsilon \leqslant 1/2$, and thus inside the band

$$\begin{aligned} \nu(\varepsilon) &= \frac{2N}{\sqrt{\mu}\hbar\omega}\sqrt{\varepsilon - \varepsilon_0}\,\theta(\mu - \mu_c), \quad \varepsilon_0 \leqslant \varepsilon < -\frac{1}{2} \\ &= \frac{N}{2\hbar\omega}\left[\left(1 - \frac{1}{\mu}\right) + \frac{2}{\sqrt{\mu}}\sqrt{\varepsilon - \varepsilon_0}\right], \quad |\varepsilon| < \frac{1}{2}. \end{aligned} \tag{17}$$

The DOS (17) in the superradiant case is shown in Fig. 1. Two particular features (discussed in detail in Sec. V) are clearly visible already. First, there is a jump of the derivative at $\varepsilon = -\frac{1}{2}$, which is a signal of a first-order ESQPT with jump discontinuity. Second, the infinite slope $\nu'(\varepsilon_0)$ at the lower band edge is due to the vanishing of one of the collective excitation modes above the ground state in the superradiant phase.

D. Dicke model in the ultrastrong-coupling limit

The limit $\mu \gg 1$ (or alternatively $\omega_0 \to 0$) for the Dicke model ($g = 0$) can be extracted from the exact results (see below), but also in a much simpler way via the polaron transformed Hamiltonian [34] with a factorizing partition sum

$$\mathcal{Z}(\beta) = \sum_{m=-N/2}^{N/2} e^{(\beta\hbar\lambda^2/N\omega)m^2} \sum_{n=0}^{\infty} e^{-\beta\hbar\omega n}. \tag{18}$$

In the semiclassical limits $N \to \infty$ and $\hbar \to 0$ we convert the sums into integrals and the DOS becomes

$$\nu(E) = \frac{N}{\hbar\omega} \int_{-1/2}^{1/2} dx\, \theta\left(\frac{E}{N} + \frac{\hbar\lambda^2}{\omega} x^2\right), \tag{19}$$

which leads to the simple square-root form

$$\nu(E) = N\left(\frac{1}{\hbar\omega} - \frac{2}{\hbar\lambda}\sqrt{\frac{-E}{N\hbar\omega}}\right), \quad E_0 \leqslant E \leqslant 0. \tag{20}$$

In this limit, the ground-state energy becomes $E_0 = -N\hbar\lambda^2/4\omega$ and the upper band edge energy $E = 0$.

IV. DICKE MODEL ($g = 0$)

In the following, we derive and discuss results for the Dicke case $g = 0$ separately because of its high relevance for the existing theoretical and experimental literature. The partition sum is obtained along the lines of the calculation in Sec. II and follows as

$$\mathcal{Z}(\beta) = \sqrt{\frac{N}{\pi\beta^3\hbar^3\omega\lambda^2}} \int_1^\infty dy \frac{\sum_\pm \pm e^{N\beta\hbar\omega_0\Phi_\pm(1/\mu, y)}}{\sqrt{y^2-1}}. \tag{21}$$

A. Low-energy excitations

We make an interesting observation in a simple analysis of $\mathcal{Z}(\beta)$ with the Laplace method [35] for $\beta N \to \infty$,

$$\mathcal{Z}(\beta) \sim \frac{e^{\beta\hbar(N\omega_0/2)}}{\beta^2\hbar^2\omega\omega_0\sqrt{1-\mu}}, \quad \mu < 1 \tag{22}$$

$$\sim 2\frac{e^{\beta\hbar(N\omega_0/4)(\mu+1/\mu)}}{\beta^2\hbar^2\omega\omega_0\sqrt{\mu^2-1}}, \quad \mu > 1. \tag{23}$$

The DOS corresponding to this asymptotic form generalizes the straight-line behavior (12) to the interacting case at low energies E and is given by

$$\nu(\varepsilon) \approx N\frac{1+\theta(\mu-1)}{\epsilon_+\epsilon_-}(\varepsilon - \varepsilon_0)\theta(\varepsilon - \varepsilon_0), \quad \varepsilon \to \varepsilon_0, \tag{24}$$

with the product $\epsilon_+\epsilon_-$ of the excitation energies coinciding with those obtained, e.g., via the Holstein-Primakov transformation [9] method. The additional factor 2 in the superradiant phase reflects the twofold degeneracy of energy levels for $N \to \infty$ [20] (see the discussion in Sec. V D).

The form (24) confirms that the low-energy behavior of the Dicke model is governed by two independent collective modes. The partition sum of the two oscillators describing these modes factorizes and as a consequence the associated DOS for excitations above the ground state with energy E_0 (including an additional degeneracy factor g_d) is

$$\nu_\mathrm{coll}(E) = g_\mathrm{d} \int dx_1 dx_2 \delta(E - x_1\epsilon_+ - x_2\epsilon_- - E_0)$$

$$= g_\mathrm{d}\frac{E - E_0}{\epsilon_+\epsilon_-}, \quad E > E_0 \tag{25}$$

as in Eq. (24) with $g_\mathrm{d} = 1$ in the normal phase and $g_\mathrm{d} = 2$ in the superradiant phase.

B. Density of states

We will give explicit analytical results for the derivative of the DOS within the band in terms of an elliptic integral below, but for the numerical evaluation it is more convenient to use the integral representation that follows from the simple Laplace back-transformation of the partition sum (21),

$$\nu(\varepsilon) = \frac{N}{\pi\hbar\omega\mu} \int_{y_0}^{y_+} dy \frac{\sqrt{(y_- - y)(y - y_+)}}{\sqrt{y^2-1}}, \tag{26}$$

with $y_\pm \equiv \mu \pm 2\sqrt{\mu}\sqrt{\varepsilon - \varepsilon_0}$ and the lower limit $y_0 \equiv y_-$ if $\varepsilon < -\frac{1}{2}$ and $y_0 \equiv 1$ if $\varepsilon > -\frac{1}{2}$ (see Appendix B).

In Fig. 1, the transition from an almost straight-line form of $\nu(\varepsilon)$ at small couplings μ in the normal phase [resembling the noninteracting case (12)] to a more complex form in the superradiant phase is clearly visible. The slope $\nu(\varepsilon)$ at the lower band edge is given by Eq. (24) and diverges at the QPT point $\mu = 1$ due to the vanishing of one of the excitation energies there [9], as expected.

The most interesting feature, however, is the signature of the ESQPT at $\varepsilon = -\frac{1}{2}$ in the superradiant phase ($\mu > 1$), a feature that was first found numerically by Pérez-Fernández and co-workers [18,19]. This nonanalyticity is only weakly visible in $\nu(\varepsilon)$ itself, but it shows very clearly in the form of a logarithmic divergence in the derivative $\nu'(\varepsilon)$ (inset). Near $\varepsilon = -\frac{1}{2}$ we find

$$\nu'(\varepsilon) \approx -\frac{\ln\frac{|\varepsilon+\frac{1}{2}|}{16(1-1/\mu)^2}}{\pi\hbar^2\omega_0\omega\sqrt{\mu-1}}, \tag{27}$$

as derived in Appendix C [also see Eq. (45)]. The origin of this feature lies in a saddle point in a classical potential landscape [18,22] (see Sec. V A).

C. Expectation values of observables

As in the LMG model [25], we can obtain averages of observables $\hat{A}$ such as the inversion J_z or the boson number $\hat{n} \equiv a^\dagger a$ as sums over eigenstates $|\alpha\rangle$ with energies E_α,

$$\langle\hat{A}\rangle(E) = \frac{1}{\nu(E)}\sum_\alpha \langle\alpha|\hat{A}|\alpha\rangle\delta(E - E_\alpha). \tag{28}$$

This can be rewritten by use of the Hellmann-Feynman theorem, which takes advantage of a parametric dependence of the E_α, i.e., $\frac{\partial E_\alpha(\lambda)}{\partial\lambda} = \langle\alpha|\frac{\partial}{\partial\lambda}\mathcal{H}|\alpha\rangle$. In our microcanonical ensemble we can now rewrite Eq. (28) as

$$\langle J_z\rangle(E) = \frac{1}{\nu(E)}\sum_\alpha \frac{\partial E_\alpha(\omega_0)}{\partial\hbar\omega_0}\delta(E - E_\alpha)$$

$$= -\frac{1}{\nu(E)}\frac{\partial}{\partial\hbar\omega_0}\int_{-\infty}^{E} dE'\nu(E') \tag{29}$$

and correspondingly for $\langle\hat{n}\rangle(E)$ with the derivative with respect to ω instead of ω_0. Note that these expressions hold for all our models (arbitrary g).

In the superradiant phase of the Dicke model ($g = 0$), this generalizes the ground-state expectation values [9]

$$\langle J_z\rangle(E_0) = -\frac{N}{2\mu}, \quad \langle\hat{n}\rangle(E_0) = \frac{N}{4}\frac{\omega_0}{\omega}\left(\mu - \frac{1}{\mu}\right) \tag{30}$$

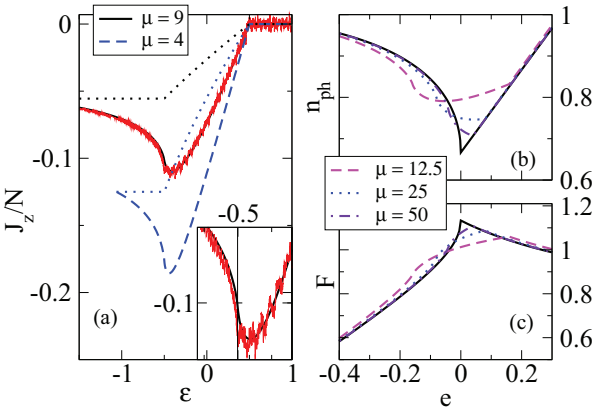

FIG. 2. (Color online) (a) Inversion $\langle J_z\rangle/N$ as a function of scaled energy $\varepsilon \equiv E/N\omega_0$ for the Dicke model ($g = 0$): analytical results from Eq. (29) and numerical data for $\mu = 9$ by Pérez-Fernández *et al.*, Fig. 2 in Ref. [19] (red fluctuating line; the inset shows a zoom near $\varepsilon = -\frac{1}{2}$). The dotted lines indicate the result (34) for the (unrestricted) Tavis-Cummings model ($g = 1$): (b) boson number n scaled with its ground state values (30) and (c) Fano factor $F \equiv \mathrm{var}(n)/n$, both as a function of scaled energy $e \equiv E/|E_0|$ for various criticality parameters μ approaching the ultrastrong-coupling regime (36) (solid black curve).

to higher energies, with Eq. (30) following from the l'Hôpital rule applied to Eq. (29),

$$\langle J_z\rangle(E_0) = -\left.\frac{\frac{\partial}{\partial\hbar\omega_0}\nu(E)}{\frac{\partial}{\partial E}\nu(E)}\right|_{E=E_0} = \frac{\partial E_0}{\partial\hbar\omega_0} \tag{31}$$

and again correspondingly for $\langle\hat{n}\rangle(E_0)$, with E_0 given in Eq. (16) [36]. Explicit expressions for the integrals needed in Eq. (29) are given in Appendix B.

Results for the inversion as a function of energy in the superradiant regime $\mu > 1$ are shown in Fig. 2(a). First, $\langle J_z\rangle(\varepsilon)$ becomes flat and levels off at exactly zero above the upper band edge $\varepsilon = \frac{1}{2}$, a feature that has already been presented in the numerical data of Pérez-Fernández *et al.* [19]. In fact, we have for arbitrary g and μ that

$$\langle J_z\rangle = 0, \quad \varepsilon \geqslant \tfrac{1}{2}, \tag{32}$$

which follows from Eq. (29), where we can extend the upper limit of the integral to ∞ for $E \geqslant \frac{N\hbar\omega_0}{2}$ because of Eq. (13) and we use $\int_{-\infty}^{\infty} dE\,\nu(E) = \mathcal{Z}(\beta = 0)$ [Eq. (4)] with the partition sum being infinite in the limit of infinite temperature but formally independent of ω_0 [see Eq. (5)].

The agreement between our analytical result and the numerical data for $j = 30$ (fluctuating red line in Fig. 2 for $\mu = 9$ [19,37]) is so good that the curves basically lie on top of each other for all energies. The data from the numerical diagonalization are obtained as an average over 20 eigenstates, but they still show quantum oscillations due to the finiteness of N (and $\hbar$). In contrast, the analytical result is based on the semiclassical limits $N \to \infty$ and $\hbar \to 0$ (with $N\hbar$ kept constant), which smear out these oscillations.

Figure 2 also shows how hard it is to directly see the logarithmic singularity at $\varepsilon = -\frac{1}{2}$ in the observable $\langle J_z\rangle$: On the scale shown in the figure, it is somewhat masked by the minimum that lies slightly above $\varepsilon = -\frac{1}{2}$. From our analytical expressions, we extract the derivative

$$\frac{\partial}{\partial\varepsilon}\langle J_z\rangle(\varepsilon) \propto \ln\left|\varepsilon + \frac{1}{2}\right| \tag{33}$$

(see Appendix B).

The logarithmic singularity is absent in the restricted Tavis-Cummings model, where instead of Eq. (33) we find that $\langle J_z\rangle(\varepsilon) = -N/(2\mu)$ is constant below the critical energy $\varepsilon = -\frac{1}{2}$, followed by a square-root nonanalyticity

$$\frac{\langle J_z\rangle(\varepsilon)}{N} = \frac{\varepsilon - \frac{1}{2}\left(\sqrt{\frac{4\varepsilon}{\mu} + \frac{1}{\mu^2} + 1} - \frac{1}{\mu}\right)}{\mu - 1 + \mu\sqrt{\frac{4\varepsilon}{\mu} + \frac{1}{\mu^2} + 1}}, \quad |\varepsilon| \leqslant \frac{1}{2}, \tag{34}$$

and a vanishing of $\langle J_z\rangle(\varepsilon)$ above the upper band edge $\varepsilon = \frac{1}{2}$ (dotted lines in Fig. 2). The nonanalyticity at the ESQPT position $\varepsilon = -\frac{1}{2}$ is consistent with the jump in the DOS derivative $\nu'(\varepsilon)$ [see Eq. (17) and the discussion in the next section].

D. Average boson number and its fluctuations

We can directly relate expectation values of the boson number $\hat{n} \equiv a^\dagger a$ and powers thereof to the Q or Husimi function $Q(\alpha;\beta) \equiv e^{-\beta\hbar\omega|\alpha|^2} Z(\alpha;\beta)$ that appears as an integrand in our partition sum $\mathcal{Z}(\beta)$ [Eq. (5)]. In the semiclassical limit, normal or antinormal ordering of operators plays no role and we can write the definition (28) as

$$\langle\hat{n}^m\rangle(E) = \frac{1}{\nu(E)}\mathcal{L}^{-1}\left[\int\frac{d^2\alpha}{\pi}|\alpha|^{2m}Q(\alpha;\beta)\right](E), \tag{35}$$

with the inverse Laplace transform of the Q function. The $|\alpha|^{2m}$ under the integral can be replaced by the operation $(-1)^m\frac{\partial^m}{\partial(\beta\hbar\omega)^m}$, which is useful to derive explicit results. For $m = 1$, we thus immediately recover the Hellmann-Feynman form (29) for $\langle\hat{n}\rangle(E)$ [division of $\mathcal{Z}(\beta)$ by β corresponds to integration over energy of $\nu(E)$]. Details for the integrals needed for $\langle\hat{n}^m\rangle(E)$, $m = 1,2$, are given in Appendix B.

The agreement between our analytical result for $\langle\hat{n}\rangle(E)$ and numerical data of Pérez-Fernández for the case $\mu = 9$ (unpublished data for $j = 15$, not shown here) is very good for all energies (numerically this requires large boson numbers for the truncated boson Hilbert space). Above the upper band edge $\varepsilon \geqslant \frac{1}{2}$, we reproduce the linear dependence in energy found by Altland and Haake via their classical Q function [12]: From Eq. (13) and the limiting value at $\varepsilon = \frac{1}{2}$ we find $\langle\hat{n}\rangle(\varepsilon) = N\frac{\omega_0}{\omega}(\frac{\mu}{6} + \varepsilon)$. Similarly, our expressions for the variance $\mathrm{var}\,\hat{n}(E) \equiv (\langle\hat{n}^2\rangle - \langle\hat{n}\rangle^2)(E)$ exactly reproduce the linear energy dependence for $\varepsilon \geqslant \frac{1}{2}$ [12] and display the macroscopic scaling with N^2 at any finite energy $E > E_0$. As expected, the ESQPT log-singularity shows up at $\varepsilon = -\frac{1}{2}$ in the mean value and the variance.

In the ultrastrong Dicke limit (20), from the partition sum (18) and Eq. (35) we derive the mean value and the variance of the scaled boson number $n \equiv \hat{n}/\langle a^\dagger a\rangle(E_0)$. At $E = E_0$, the variance vanishes as our calculation only accounts for the leading terms $\propto N^2$ and is not sensitive to subleading

dependences $\propto N$ [38]. We find

$$\begin{aligned} n(e<0) &= \frac{\frac{2}{3}+e+\frac{1}{3}(-e)^{3/2}}{1-\sqrt{-e}}, \\ \mathrm{var}\, n(e<0) &= \frac{1}{5}[(1+\sqrt{-e})(6+4e)+e^2]-n^2, \\ n(e>0) &= \frac{2}{3}+e, \quad \mathrm{var}\, n(e>0) = \frac{34}{45}+\frac{2}{3}e, \end{aligned} \tag{36}$$

with the energy variable $e \equiv E/|E_0| > -1$ scaled with the ground-state energy E_0. Figures 2(b) and 2(c) clearly show Eq. (36) as the limiting form for the scaled boson number n and the Fano factor $F \equiv \mathrm{var}\, n/n$ when μ increases to large values in the superradiant regime.

V. GENERALIZED DICKE MODELS ($g \geqslant 0$)

We now turn to the general case of arbitrary $0 \leqslant g \leqslant 1$ in our model Hamiltonian $\mathcal{H}$ [Eq. (1)].

A. Classical potential

As we are dealing with a mean-field Hamiltonian in the thermodynamic limit $N \to \infty$, all critical features are expected to be related to extremal points in a classical potential landscape [22]. In fact, the following very simple analysis of potential extrema is very helpful for interpreting the various critical regions following from the exact expressions for the DOS derivative $\nu'(E)$ in terms of elliptic integrals.

The partition sum $\mathcal{Z}(\beta)$ [Eq. (5)] contains a potential in a natural way: After carrying out the angular momentum trace, we can write it as phase-space integral

$$\begin{aligned} \mathcal{Z}(\beta) &= \frac{N}{\pi\beta\hbar\omega}\int dx\, dp \frac{\sum_\pm \pm e^{-\beta N\hbar\omega_0 U_\pm(x,p)}}{\sqrt{1+\mu(x^2+p^2)}}, \\ U_\pm(x,p) &\equiv \frac{1}{4}(x^2+p^2) \mp \frac{1}{2}\sqrt{1+\mu(x^2+g^2p^2)}. \end{aligned} \tag{37}$$

The contribution relevant for the region $\varepsilon \leqslant \frac{1}{2}$ below the upper band edge of the DOS is the plus part, i.e., U_+, whereas the minus part, i.e., U_-, only contributes to $\varepsilon \geqslant \frac{1}{2}$ in $\nu(\varepsilon)$ leading to the leveling off at the constant oscillator DOS [see Eq. (13)].

The extrema of the (dimensionless) potential $U_+(x,p)$ have a simple structure. We only discuss the superradiant phase $\mu \geqslant 1$, which is of interest for the ESQPT. For all g there are two minima at $(x = \pm\sqrt{\mu - 1/\mu}, p = 0)$, where $U(x,p) = \varepsilon_0$ [the scaled ground-state energy (16) as expected], and an extremum at $(x = 0, p = 0)$, where $U(x,p) = -1/2$, the scaled ESQPT critical energy. For $g < \frac{1}{\sqrt{\mu}}$, the extremum $(x = 0, p = 0)$ is a saddle point leading to logarithmic nonanalyticities in $\nu(\varepsilon)$ as we already saw in the Dicke case $g = 0$.

In contrast, for $g > \frac{1}{\sqrt{\mu}}$, the saddle point at $(x = 0, p = 0)$ is transformed into a local maximum and instead two new saddle points at finite momenta $(x = 0, p = \pm\sqrt{g^2\mu - 1/g^2\mu})$ appear where $U(x,p) = \varepsilon_g$ with the energy ε_g (again scaled by $N\hbar\omega_0$) given by

$$\varepsilon_g \equiv -\frac{1}{4}\left(g^2\mu + \frac{1}{g^2\mu}\right). \tag{38}$$

As we will see below, this leads to a logarithmic-type ESQPT in $\nu'(\varepsilon)$ at $\varepsilon = \varepsilon_g$, in addition to a nonanalyticity at $\varepsilon = -1/2$ that is now a first-order jump discontinuity-type ESQPT.

Finally, at $g = 1$ (restricted Tavis-Cummings model), the potential becomes a sombrero function with only one local maximum at $(x = 0, p = 0)$ and a continuous ring of minima where again $U(x,p) = \varepsilon_0$. We emphasize that this Goldstone mode appears for all couplings $\mu > 1$ in the superradiant phase and not only at criticality [27]. Its origin lies in the gauge symmetry $a \to ae^{i\phi}$, $J_+ \to e^{-i\phi}J_+$ of the Hamiltonian $\mathcal{H}$, which is in rotating-wave form at $g = 1$. In the normal phase, $\langle a\rangle$ and $\langle J_+\rangle$ vanish and this symmetry does not play a big role, in contrast to the superradiant phase where both expectation values become macroscopic.

As a consequence, for $g = 1$, one of the collective excitation energies in the superradiant phase vanishes, as we also directly confirmed using the equation-of-motion method by Bhaseen *et al.* [7]. This is the reason for the divergence of $\nu'(\varepsilon)$ at the lower band edge $\varepsilon = \varepsilon_0$, as we already observed in Eq. (17) and Fig. 1. In contrast, for $g < 1$ one has a nondiverging $\nu'(\varepsilon_0)$ [see Eq. (24) for the Dicke case $g = 0$].

B. Exact expressions for $\nu'(\varepsilon)$

We now turn to the full exact solution for arbitrary $0 \leqslant g \leqslant 1$. Instead of trying a direct evaluation of the DOS $\nu(\varepsilon)$ [Eq. (11)] (which is cumbersome due to the step function), progress is made by calculating the derivative $\nu'(\varepsilon)$, for which we obtain the expression

$$\begin{aligned} \nu'(\varepsilon) &= \frac{1}{4\pi\hbar^2\lambda^2 g}\int_1^\infty dy \int_0^{2\pi} d\varphi \sum_\pm \pm\delta(\varepsilon + \Phi_\pm(\alpha(\varphi), y)) \\ &= -\frac{1}{2\pi\hbar^2\lambda^2 g}\sum_\pm \pm \mathrm{Im}\int_1^\infty \\ &\quad \times \frac{dy}{\sqrt{\varepsilon + i0 + \Phi_\pm(\mu^{-1}, y)}\sqrt{\varepsilon + i0 + \Phi_\pm(g^{-2}\mu^{-1}, y)}} \end{aligned} \tag{39}$$

with $\Phi_\pm$ defined in Eq. (8) and where we used $-\pi\delta(x) = \mathrm{Im}\, 1/(x + i0)$ and Eq. (15).

To evaluate Eq. (39) we first recall that only the plus term in the $\sum_\pm$ contributes within the band $[\varepsilon_0, \frac{1}{2}]$ [see the remark after Eq. (14)]. Next we use $\sqrt{x + i0} = \sqrt{x}\theta(x) + i\sqrt{-x}\theta(-x)$ to rewrite Eq. (39) within the band as

$$\nu'(\varepsilon) = \frac{1}{2\pi\hbar^2\lambda^2 g}\int_1^\infty \frac{dy\, \theta(\varepsilon - p(y))\theta(q(y) - \varepsilon)}{\sqrt{-[\varepsilon - p(y)][\varepsilon - q(y)]}}, \tag{40}$$

where we defined the two parabolas $p(y) \equiv -\Phi_+(\mu^{-1}, y)$ and $q(y) \equiv -\Phi_+(g^{-2}\mu^{-1}, y)$ between which the energy ε has to lie. This determines the boundaries of the y integral, expressed in terms of the zeros of $p(y)$ and $q(y)$,

$$y_\pm \equiv \mu \pm 2\sqrt{\mu}\sqrt{\varepsilon - \varepsilon_0}, \tag{41}$$

$$z_\pm \equiv g^2\mu \pm 2\sqrt{g^2\mu}\sqrt{\varepsilon - \varepsilon_g}. \tag{42}$$

In the superradiant phase ($\mu > 1$), by considering $p(y) < \varepsilon < q(y)$ we find two regimes depending on the value of the parameter g. For $g^2\mu < 1$, for energies $\varepsilon \leqslant -\frac{1}{2}$ the boundaries are $[y_-, y_+]$. In contrast, for $g^2\mu > 1$ there are two regions:

one with boundaries $[y_-, y_+]$ if $\varepsilon \leqslant \varepsilon_g$ and the other for energies $\varepsilon_g \leqslant \varepsilon \leqslant -\frac{1}{2}$ with $y_- \leqslant z_- \leqslant z_+ \leqslant y_+$ and two intervals $[z_+, y_+]$ and $[y_-, z_-]$ contributing to the y integral. Furthermore, for all values of g and μ and for energies $\varepsilon \geqslant -\frac{1}{2}$, the boundaries are $[z_+, y_+]$ with $z_- \leqslant y_- \leqslant z_+ \leqslant y_+$. We also note that for $\varepsilon \leqslant \varepsilon_g$, the $z_\pm$ become complex.

This now allows us to give explicit expressions for $\nu'(\varepsilon)$ [39]:

$$\nu'(\varepsilon) = \frac{4}{\pi\hbar^2\omega\omega_0}\frac{1}{\sqrt{p_+ p_-}} K\left(\frac{(y_+ - y_-)^2 - (p_+ - p_-)^2}{4p_+ p_-}\right) \quad \text{for} \quad \varepsilon_0 \leqslant \varepsilon \leqslant \varepsilon_g, \tag{43a}$$

$$\nu'(\varepsilon) = \frac{4}{\pi\hbar^2\omega\omega_0} \begin{cases} \frac{2}{\sqrt{(y_+ - z_-)(z_+ - y_-)}} K\left(\frac{(y_+ - z_+)(z_- - y_-)}{(y_+ - z_-)(z_+ - y_-)}\right), & g^2\mu \geqslant 1 \\ \frac{1}{\sqrt{(y_+ - z_+)(y_- - z_-)}} K\left(\frac{(y_+ - y_-)(z_+ - z_-)}{(y_+ - z_+)(y_- - z_-)}\right), & g^2\mu \leqslant 1 \end{cases} \quad \text{for} \quad \varepsilon_g \leqslant \varepsilon \leqslant -\frac{1}{2}, \tag{43b}$$

$$\nu'(\varepsilon) = \frac{4}{\pi\hbar^2\omega\omega_0}\frac{1}{\sqrt{(y_+ - y_-)(z_+ - z_-)}} K\left(\frac{(y_+ - z_+)(y_- - z_-)}{(y_+ - y_-)(z_+ - z_-)}\right) \quad \text{for} \quad -\frac{1}{2} \leqslant \varepsilon \leqslant \frac{1}{2}. \tag{43c}$$

Here $y_\pm$ and $z_\pm$ have already been defined in Eq. (41),

$$p_\pm \equiv \sqrt{(g^2\mu - y_\pm)^2 + 4g^2\mu(\varepsilon_g - \varepsilon)}, \tag{44}$$

and $K(m) \equiv \int_0^{\pi/2} d\varphi (1 - m\sin^2\varphi)^{-1/2}$ denotes the elliptic integral of the first kind. Note that for the normal phase $\mu < 1$ only Eq. (43c) is relevant.

C. The ESQPT for $0 \leqslant g \leqslant 1$

Figure 3 (left) displays the main features contained in our expressions (43) in the superradiant phase. At small $g < 1/\sqrt{\mu}$, only the logarithmic-type singularity appears at $\varepsilon = -\frac{1}{2}$, reflecting the ESQPT that we already saw in the Dicke ($g = 0$) case and anticipated from the discussion of the potential (37). Writing the scaled energy $\varepsilon = -\frac{1}{2} + \delta$ with small δ, from our exact expressions for $\nu'(\varepsilon)$ we explicitly extract (Appendix B) the logarithmic divergence

$$\nu'\left(-\frac{1}{2} + \delta\right) \approx \frac{-\ln\left|\frac{r}{16}\delta\right|}{\pi\hbar^2\omega\omega_0\sqrt{(\mu - 1)(1 - g^2\mu)}} \tag{45}$$

with the constant r defined in Eq. (C3).

This situation changes for larger $g > 1/\sqrt{\mu}$, where the singularity at $\varepsilon = -\frac{1}{2}$ becomes a jump-type discontinuity with a jump by a factor of 2,

$$\nu'\left(\varepsilon = -\frac{1}{2} \pm 0^+\right) = \frac{3 \mp 1}{2\hbar^2\omega\omega_0\sqrt{(\mu - 1)(g^2\mu - 1)}}. \tag{46}$$

In addition, the logarithmic-type ESQPT singularity has now moved to the position $\varepsilon = \varepsilon_g$ corresponding to the two new saddle points in the potential landscape $U_+(x, p)$.

In the limit $g = 1$, from Eq. (43) we recover the Tavis-Cummings result (17): When pushed against the lower band edge ε_0, all that remains from the logarithmic singularity is a square-root divergence, which (as discussed above) can be traced back to the Goldstone mode of the rotating-wave-approximation model in the superradiant phase. Another check is the ultrastrong Dicke ($g = 0$) limit (20) that follows from Eq. (43) for $\omega_0 \to 0$.

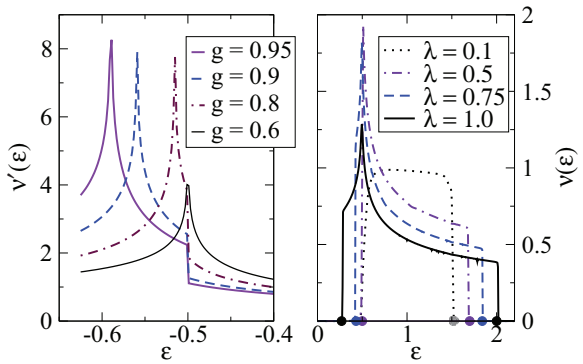

FIG. 3. (Color online) On the left is the DOS derivative $\nu'(\varepsilon)$ [Eq. (43)] as a function of scaled energy $\varepsilon \equiv E/N\hbar\omega_0$ for generalized Dicke models in the superradiant phase for various values of g [Eq. (1)] and criticality parameter $\mu = 2$. On the right is the DOS for the Tavis-Cummings model (55) restricted to excitation number $N_{\text{ex}} = N$ [see Eq. (3)] and frequencies $\omega = 2$ and $\omega_0 = 1$ for various coupling parameters λ. The solid dots on the ε axis indicate the values of the band edges for the respective values of λ in the numerical data in Fig. 4 of Ref. [18].

D. Collective excitations and degeneracies

In the normal phase $\mu < 1$ and again in analogy with the Dicke case, we confirm the low-energy behavior

$$\nu'\left(\varepsilon = -\frac{1}{2}\right) = \frac{1}{\epsilon_+\epsilon_-} = \frac{1}{\hbar^2\omega\omega_0\sqrt{(\mu - 1)(g^2\mu - 1)}} \tag{47}$$

at arbitrary $0 \leqslant g \leqslant 1$ with the collective low-energy excitation energies $\epsilon_\pm$. We checked that Eq. (47) also follows from the diagonalization of our Hamiltonian $\mathcal{H}$ [Eq. (1)] via a Bogoliubov transformation (Appendix D) or alternatively as the determinant of the Jacobian belonging to the normal-phase fixed point in the classical equation-of-motion method [7].

In the superradiant phase $\mu > 1$, we directly find from Eq. (43), using $y_\pm = \mu$ at $\varepsilon = \varepsilon_0$, that at the lower band edge

$$\nu'(\varepsilon_0) = \frac{2}{\epsilon_+\epsilon_-} = \frac{2}{\hbar^2\omega\omega_0\sqrt{(1-g^2)(\mu^2-1)}}. \tag{48}$$

Again we recover the divergence of $\epsilon_+\epsilon_-$ at $g = 1$ (Tavis-Cummings model) and our Dicke result for $g = 0$ [Eq. (24)].

At the upper band edge $\varepsilon = +\frac{1}{2}$, in contrast, we have $y_- = z_- = -1$, $y_+ = 1 + 2\mu$, and $z_+ = 1 + 2g^2\mu$ and thus from Eq. (43)

$$\nu'\left(\frac{1}{2}\right) = \frac{1}{\hbar^2\omega\omega_0\sqrt{(1+\mu)(1+g^2\mu)}}. \tag{49}$$

Both forms (47) and (48) are consistent with the general form of the low-energy behavior of the model described by two collective modes with energies $\epsilon_\pm$, i.e., $\nu'(\varepsilon) \to g_\mathrm{d}/\epsilon_+\epsilon_-$ at the lower band edge both in the normal and in the superradiant phase, where g_d is the level degeneracy factor [see Eq. (25)]. Note that the classical potential (37) has $g_\mathrm{d} = 2$ equivalent minima at $\mu > 1$, which is of course consistent with the *two* effective Hamiltonians describing the superradiant phase at low energies [9]. Here the Tavis-Cummings case ($g = 1$) can be formally interpreted as having degeneracy $g_\mathrm{d} = \infty$.

At this point, an interesting comparison can be made with recent numerical results by Puebla, Relaño, and Retamosa [20], who found that in the superradiant phase, the energy levels in the Dicke model ($g = 0$) are doubly degenerate ($g_\mathrm{d} = 2$) below the ESQPT critical energy $\varepsilon = -\frac{1}{2}$ and nondegenerate ($g_\mathrm{d} = 1$) above that energy. In the normal phase, in contrast, they found no degeneracy at any energy.

Our results above only refer to energies at the band edges, but they are consistent with this picture and generalize it to models with $g \geqslant 0$. In particular, the upper-band-edge value (49) holds for all values of the criticality parameter μ, in agreement with the absence of degeneracy at large energies found in Ref. [20].

E. Comparision with the LMG model

As mentioned in the Introduction, our results bear close analogies to the extensive studies of Ribeiro, Vidal, and Mosseri [24,25] for the LMG model,

$$\mathcal{H} = -\frac{1}{N}\left(\gamma_x J_x^2 + \gamma_y J_y^2\right) - hJ_z, \tag{50}$$

where in the γ_y-γ_x phase diagrams four different phases were identified. Nonanalyticities in the DOS $\nu(E)$ and the integrated DOS were related to extremal points in the classical potential landscape belonging to Eq. (50) (see our analysis in Sec. V A) and analytical expressions in terms of elliptic integrals followed via a mapping to a first-order nonlinear differential equation.

For the Dicke-type models (1), due to the additional boson degree of freedom, the derivative $\nu'(E)$ of the level density [rather than $\nu(E)$ itself] is the key quantity in the analysis, but otherwise we have a clear correspondence. First, in the normal (symmetric) phase both models have smooth level densities. Next, the single-logarithmic-divergence phase of the LMG model (phase II in Ref. [25] with $|\gamma_y| < h < \gamma_x$) corresponds to the case $g^2\mu \leqslant 1$ in the Dicke models, whereas the single-logarithmic-jump phase of the LMG model (phase IV in Ref. [25] with $h < \gamma_y < \gamma_x$) corresponds to the case $g^2\mu \geqslant 1$ in the Dicke-type models. In this latter phase, we obtain the same factor of 2 jump discontinuity as [25] [see Eq. (43)], but with our method we cannot further analyze the spectral subtleties there since we have no access to, e.g., the energy difference between two consecutive levels. Also note that we have only considered positive couplings in Eq. (1), which is why there is no analogon to the phase III [25] with two logarithmic divergences in the LMG model.

Finally, the isotropic LMG model ($\gamma_y = \gamma_x$) is easily solvable in term of J_z eigenstates only and it has a single Goldstone mode [40]. In this limit, the LMG model corresponds to the (unrestricted) Tavis-Cummings Hamiltonian ($g = 1$) [see Eq. (17) and Sec. V A].

VI. RESTRICTED TAVIS-CUMMINGS MODEL

Finally, we turn to the Tavis-Cummings model ($g = 1$) including the restriction defined by a fixed value of the conserved excitation number N_ex [Eq. (3)]. Pérez-Fernández *et al.* found a ground-state QPT determined by the condition $\lambda > |\omega_0 - \omega|/2$ and an ESQPT in the form of a strongly increased level density at $\varepsilon \equiv E/N\hbar\omega_0 = +\frac{1}{2}$ and a needlelike singularity of the observable $\langle J_z\rangle$ at that energy [18]. Unfortunately and somewhat ironically, in contrast to a numerical analysis, the additional conserved quantity N_ex in the restricted Tavis-Cummings case $g = 1$ makes it much harder to make analytical progress (when compared to all other models for $0 \leqslant g \leqslant 1$ including the Dicke case $g = 0$).

In our method based on the partition sum, $\mathcal{Z}(\beta)$ now has to be carried out at fixed N_ex, a condition that can be included in the angular momentum trace part (5) in the form of a δ function reflecting Eq. (3) (see Appendix A), leading to

$$\mathcal{Z}(\beta) = \sum_{mm'} \exp\left(-\beta\hbar m'\sqrt{\omega_0^2 + \frac{4\lambda^2}{N}(K-m)}\right) \times e^{-\beta\hbar\omega(K-m)}|d_{mm'}(\theta)|^2, \tag{51}$$

where $K \equiv N_\mathrm{ex} - N/2$,

$$d_{mm'}(\theta) \equiv \langle m|e^{-i\theta J_y}|m'\rangle \tag{52}$$

is a rotation matrix element (Wigner's d function) [41], and the angle θ is defined by

$$\cos\theta = \frac{1}{\sqrt{1 + \frac{4\lambda^2}{N\omega_0^2}(K-m)}}. \tag{53}$$

As we are interested in the $N \equiv 2j \to \infty$ limit only, we use the semiclassical approximation for the rotation matrix element [41,42],

$$|d_{mm'}(\theta)|^2 \approx \frac{1}{\pi}[j^2\sin^2\theta - m^2 - m'^2 + 2mm'\cos\theta]^{-1/2}, \tag{54}$$

which holds for positive arguments of the square root and where $|d|^2$ is approximated by zero otherwise.

After converting the m sums into integrals using $m \equiv Nx$ and $m' \equiv Nx'$, this leads to

$$\nu(\varepsilon) = N \int_{-1/2}^{1/2} dx \frac{\theta\left(\frac{1}{2} - |x'|\right)}{\hbar\sqrt{\omega_0^2 + 4\lambda^2\left(\frac{K}{N} - x\right)}} |d_{Nx,Nx'}(\theta)|^2,$$
$$x' \equiv \frac{\varepsilon/\hbar - \omega\left(\frac{K}{N} - x\right)}{\sqrt{\omega_0^2 + 4\lambda^2\left(\frac{K}{N} - x\right)}}. \tag{55}$$

Note that in contrast to the DOS in the unrestricted cases discussed above, $\nu(\epsilon)$ is of order $N^0 = 1$ and thus not proportional to N (the factor N cancels with $1/N$ from the Wigner d function at large N). This corresponds to the reduction of dimensionality of the model due to the additional conserved quantity $N_{\rm ex}$ and is best visualized in a lattice representation of our model $\mathcal{H}$ [Eq. (1)], where each point of the lattice represents a basis state $|jm\rangle \otimes |n\rangle$ [10]. The rotating-wave-approximation version $g = 1$, i.e., the Tavis-Cummings model, then decomposes into independent parallel chains that can be labeled by $N_{\rm ex}$ and become one-dimensional lines in the thermodynamic limit, whereas the full lattice is two dimensional.

Results for the DOS $\nu(\varepsilon)$ for the restricted Tavis-Cummings model with conserved quantity $K = N/2$ ($N_{\rm ex} = N$), $\omega_0 = 1$, and $\omega = 2$ are shown in Fig. 3. For small λ, $\nu(\varepsilon)$ essentially has the shape of the uncoupled case where

$$\nu(\varepsilon) = \frac{\theta\left(\frac{1}{2} - \left|\frac{\varepsilon/\hbar - \omega/2}{\omega_0 - \omega}\right|\right)}{\hbar|\omega_0 - \omega|}, \tag{56}$$

which follows from the partition sum (51) for $\lambda = 0$ and $d_{mm'}(\theta) = \delta_{mm'}$. At finite λ, we did not find a simple analytical form for the band edges of $\nu(\varepsilon)$, but their numerical values following from Eq. (55) agree well with the results from exact numerical diagonalizations by Pérez-Fernández *et al.* [18].

In a similar way, we find a logarithmic singularity in $\nu(\varepsilon)$ at $\varepsilon = \frac{1}{2}$ for $\lambda > \lambda_c$, in agreement with the needlelike singularity of $\langle J_z\rangle$ found in Refs. [18,43]: Expanding the argument of the d function (54) below the upper integration limit $x = \frac{1}{2}$, we find a purely quadratic behavior

$$\frac{\sin^2\theta}{4} - x^2 - x'^2 + 2xx'\cos\theta \approx (-1 + 4\lambda^2)\left(x - \frac{1}{2}\right)^2 \tag{57}$$

with no constant or linear term at $\varepsilon = \frac{1}{2}$ and thus $|d_{Nx,Nx'}(\theta)|^2 \propto |x - \frac{1}{2}|^{-1}$, which upon integration leads to the logarithmic form for $\lambda > 0.5$ there.

VII. CONCLUSION

In all of our calculations, we have only considered the semiclassical limit for which the partition sum $\mathcal{Z}(\beta)$ and thereby the DOS can be obtained without further approximations. Importantly, in order to arrive at our results we had to keep the full angular momentum character of the model, i.e., we did not make any kind of expansion using Holstein-Primakov bosons [9,10]. The close analogy to results for the LMG model [25] suggests an equivalence between the LMG and Dicke models not only for canonical thermodynamics [44] but also for the abnormal microcanonical situation relevant for ESQPTs [45].

For finite N, an obvious next task would be to extract finite-size scaling exponents [46–48] for the ESQPT (see recent numerical results for the Dicke $g = 0$ case [20]) or a $1/N$ expansion similar to the LMG [24,25] model.

The Hellmann-Feynman theorem (29) links the ESQPT nonanalyticities to observables (or in fact the QPT order parameters), which might be more relevant for possible experiments than the DOS itself. Here our analysis has remained incomplete in that we have only focused on the Dicke ($g = 0$) case. In the $g > 0$ case, the analytical evaluation of $\langle J_z\rangle$ is in principle straightforward, but for a comparison with the regime in which spectral subtleties similar to the LMG model [25] are expected one would have to put forth quite some numerical effort in addition. Another open point is the calculation of angular momentum observables (such as J_x) that cannot directly be obtained via the Hellmann-Feynman theorem.

An essential condition for the ESQPT in the Dicke models is the restriction to the Dicke states $|jm\rangle$ with maximum $j = N/2$ in order to avoid the usual high degeneracy, i.e., the entropy term in $\mathcal{Z}(\beta)$ that leads to completely different physics, i.e., a thermal phase transition. In the ultrastrong-coupling limit $\lambda \to \infty$ of the Dicke ($g = 0$) model, we have recently discussed [34] a realization of such a restriction with bosons, where the partition sum does not contain the combinatorial degeneracy factor of the usual fermionic (spin-$\frac{1}{2}$) Dicke case and as a result, the thermal phase transition does not occur. An interesting option therefore would be to use bosons and to directly explore the properties related to the thermodynamic ensemble defined by our canonicial partition sum (5). In principle, one could then try to directly reconstruct ESQPT properties from equilibrium quantities at finite temperatures.

A further point is the peculiar character of the models where ESQPTs have been studied so far. The Dicke or LMG models (which correspond to zero-dimensional field theories) are special in that there is no intrinsic length scale (like in lattice spin models). In the thermodynamic limit, mean-field theory becomes exact and the ground-state QPTs always follow some (classical) bifurcation scenario, on top of which one has nontrivial finite-size corrections. A next step would therefore be to investigate ESQPTs in generic many-body systems in an expansion around a mean-field approximation (see [49] for a recent study of metastable QPT in a one-dimensional Bose gas).

We also emphasize that the DOS $\nu(E)$ relevant for ESQPTs is different from the usual single-quasiparticle excitation density of states known from, e.g., optical excitation spectra in many-body systems (see [50] for a recent example in the Bose-Hubbard Hamiltonian). Nevertheless, it would be worth investigating the relation between the two quantities (be it only on a technical level) for further models in detail, in particular in view of the band-structure character of our calculation above.

Finally, we comment on possible experimental realizations of ESQPTs in Dicke models. Quantum quenches [18,20] seem to be a promising possibility to convert the singular energetic features into the time domain. The ground-state QPT has been experimentally tested for both the Dicke-Hepp-Lieb [1] and the LMG [51] models in Bose-Einstein condensates. One

challenge, as mentioned above, is to stay within the relevant subspaces of states (e.g., the Dicke states with $j = N/2$) when implementing the effective Hamiltonian $\mathcal{H}$ [Eq. (1)] for a real physical system.

ACKNOWLEDGMENTS

I thank P. Pérez-Fernández for discussions on ESQPTs, for providing the original numerical data from Fig. 2 in Ref. [19] for the inversion $\langle J_z\rangle$, and for showing me his unpublished data from new numerical calculations for the photon number $\langle a^\dagger a\rangle$ in the Dicke model. I am also indebted to C. Emary, A. Relaño, and P. Ribeiro for valuable comments on this manuscript, and I acknowledge support by the DFG via Projects No. BR 1528/7-1, No. BR 1528/8-1, and No. SFB 910.

APPENDIX A: ANGULAR MOMENTUM TRACE

We evaluate the angular momentum trace $Z(\alpha;\beta) \equiv \mathrm{Tr} e^{-\beta H_g}$ in Eq. (5) by writing $\alpha = x + ip$ and

$$H_g \equiv \hbar\omega_0 J_z + \frac{2\hbar\lambda}{\sqrt{N}}(xJ_x - gpJ_y). \tag{A1}$$

We carry out the trace by unitarily rotating the angular momentum, first rotating around the J_z axis via

$$\gamma_1(-J_y\sin\phi + J_x\cos\phi) = e^{i\phi J_z}\gamma_1 J_x e^{-i\phi J_z} \tag{A2}$$

with parameters $\gamma_1\sin\phi = gp\frac{2\lambda}{\sqrt{N}}$ and $\gamma_1\cos\phi = x\frac{2\lambda}{\sqrt{N}}$ after which we rotate the resulting $\omega_0 J_z + \gamma_1 J_x$ around J_y, using

$$\gamma(-J_x\sin\theta + J_z\cos\theta) = e^{i\theta J_y}\gamma J_z e^{-i\theta J_y} \tag{A3}$$

and identifying $\omega_0 = \gamma\cos\theta$ and $-\gamma\sin\theta = \gamma_1$. The resulting exponent in the trace is now diagonal,

$$Z(\alpha;\beta) = \mathrm{Tr} e^{-\beta\hbar\gamma J_z} = \sum_{m=-N/2}^{N/2} e^{-\beta m\gamma} \tag{A4}$$

with the frequency $\gamma = \sqrt{\gamma_1^2 + \omega_0^2}$ given by

$$\gamma = \omega_0\sqrt{1 + \frac{4\lambda^2}{N\omega_0^2}(x^2 + g^2p^2)}. \tag{A5}$$

Note that we can use either the positive or negative square root for γ as the sum is symmetric in m. For large $N\to\infty$, we can neglect the difference between N and $N+1$ to write $Z(\alpha;\beta) = \sum_\pm \pm e^{\pm\beta\gamma\hbar N/2}/(e^{\beta\hbar\gamma} - 1)$. In the semiclassical limit $\beta\hbar\omega_0 \to 0$ this becomes $\sum_\pm \pm e^{\pm\beta\gamma\hbar N/2}/\beta\hbar\gamma$, a result that one also obtains by replacing the sum (A4) by the integral $N\int_{-1/2}^{1/2} dm\, e^{-\beta N m\hbar\gamma}$. Rescaling of the integration variables $\tilde{x} \equiv x/\sqrt{N}$ and $\tilde{p} \equiv gp/\sqrt{N}$, introducing polars, and defining $y \equiv \sqrt{1 + \frac{4\lambda^2}{\omega_0^2}r^2}$ now leads to Eq. (7).

For the Tavis-Cummings model ($g = 1$) discussed in Sec. VI, the partition sum is restricted by a conserved excitation number N_{ex}, which is included in the angular momentum trace in the form of a δ function,

$$Z_{\mathrm{TC}} \equiv \mathrm{Tr}[\delta(K - |\alpha|^2 - J_z)e^{-\beta H_g}], \tag{A6}$$

with the same H_g [Eq. (A1)] and $K \equiv N_{\mathrm{ex}} - N/2$. Again, we first rotate the exponential by an angle ϕ around the J_z axis as above, but the second rotation by the angle θ around the J_y axis does not commute with J_z in the δ function and therefore

$$Z_{\mathrm{TC}} = \mathrm{Tr}[\delta(K - |\alpha|^2 - J_z)e^{i\theta J_y}e^{-\beta\hbar\gamma J_z}e^{-i\theta J_y}] \tag{A7}$$

with γ given by Eq. (A5) for $g = 1$. Here the angle θ is given by

$$\cos\theta = \frac{1}{\sqrt{1 + \frac{4\lambda^2}{N\omega_0^2}|\alpha|^2}}. \tag{A8}$$

The trace can be done explicitly by inserting a complete set of Dicke states $|jm\rangle$, leading to

$$Z_{\mathrm{TC}} = \sum_{mm'}\delta(K - |\alpha|^2 - m)|d_{mm'}(\theta)|^2 e^{-\beta\hbar\gamma m'}, \tag{A9}$$

where the matrix element $d_{mm'}$ is Wigner's d function (52). Inserting into Eq. (5) and carrying out the α integral then yields Eq. (51).

APPENDIX B: DICKE MODEL

The DOS in the Dicke case ($g = 0$) follows from the Laplace back-transformation of the partition sum (21) by use of

$$\mathcal{L}^{-1}[\beta^{-3/2}e^{-\beta\Omega}](E) = \frac{2}{\sqrt{\pi}}\sqrt{E-\Omega}\,\theta(E-\Omega) \tag{B1}$$

and writing $\mathrm{Re}\sqrt{x + i0} = \sqrt{x}\theta(x)$ (which is convenient for some of the following transformations),

$$\nu(\varepsilon) = \frac{2N}{\pi\sqrt{\mu}\omega}\mathrm{Re}\sum_\pm \pm\int_1^\infty dy\frac{\sqrt{\varepsilon + i0 + \Phi_\pm\left(\frac{1}{\mu},y\right)}}{\sqrt{y^2-1}}. \tag{B2}$$

Within the band, the explicit evaluation of the step function leads to Eq. (26).

Next and again within the band, the mean inversion follows from Eq. (29) as

$$\langle J_z\rangle = -\frac{N^2}{2\pi\hbar\omega\mu\nu(\varepsilon)}I_-^{1/2}, \tag{B3}$$

where we defined the integrals (that we numerically evaluate to obtain the curves in Fig. 2)

$$I_\sigma^\alpha \equiv \int_{y_0}^{y_+}\frac{\sigma\frac{y^2-1}{\mu} + y}{\sqrt{y^2-1}}[(y_- - y)(y - y_+)]^\alpha dy, \tag{B4}$$

with the sign $\sigma = \pm$, $\alpha = \pm\frac{1}{2}$, and the lower limit

$$y_0 = y_-, \quad \varepsilon \leqslant -\frac{1}{2}; \quad y_0 = 1, \quad \varepsilon \geqslant -\frac{1}{2}; \tag{B5}$$

and $y_\pm \equiv \mu \pm 2\sqrt{\mu}\sqrt{\varepsilon - \varepsilon_0}$. At $\varepsilon = \frac{1}{2}$ we find $I_-^{1/2} = 0$ and thus $\langle J_z\rangle = 0$ [see Eq. (32)].

In the vicinity of the ESQPT, we write $\varepsilon = -\frac{1}{2} + \delta$. For $\delta\to 0$, we find $\frac{\partial}{\partial\omega_0}\nu(\varepsilon) \approx \frac{1}{4}\nu'(\varepsilon)$ with the logarithmic singularity (27) [see also Eq. (45)] and as a consequence the derivative of $\langle J_z\rangle(\varepsilon)$ is given by

$$\frac{\partial}{\partial\varepsilon}\langle J_z\rangle(\varepsilon) = -\frac{\frac{\partial}{\partial\varepsilon}\nu(\varepsilon)\langle J_z\rangle(\varepsilon) + \frac{\partial}{\partial\omega_0}\nu(\varepsilon)}{\nu(\varepsilon)} \propto \ln|\delta|, \tag{B6}$$

with $\frac{\partial}{\partial\omega_0}\nu(E) = \frac{N}{2\pi\omega\omega_0} I_-^{-1/2}$. As we checked numerically, the logarithmic singularity near $\varepsilon = -\frac{1}{2}$ in Eq. (B6) has a prefactor that (depending on the value of μ) is either positive or negative.

For the boson number $\hat{n}$, we used the Hellmann-Feynman theorem to find the first moment

$$\langle\hat{n}\rangle(\varepsilon) = \frac{N\omega_0}{\omega}\left(\frac{\varepsilon}{3} + \frac{N}{6\pi\mu\hbar\omega\nu(\varepsilon)} I_+^{1/2}\right), \quad \varepsilon \leqslant \frac{1}{2} \tag{B7}$$

and the linear form [12] $\langle\hat{n}\rangle(\varepsilon) = N\frac{\omega_0}{\omega}(\frac{\mu}{6} + \varepsilon)$ for $\varepsilon \geqslant \frac{1}{2}$, where the constant follows from $I_+^{1/2} = \pi\mu(2+\mu)$ at $\varepsilon = \frac{1}{2}$. We obtain the second moment via Eq. (35) by Laplace back-transformation and carrying out the integration

$$\langle\hat{n}^2\rangle(\varepsilon) = \left(\frac{N\omega_0}{\omega}\right)^2 \frac{N}{\pi\hbar\omega\nu(\varepsilon)}\left[\frac{J_2^{1/2}}{\mu} + \frac{J_0^{5/2}}{80\mu^3} + \frac{J_1^{3/2}}{6\mu^2}\right], \tag{B8}$$

where we defined the integrals (to be solved numerically)

$$J_\sigma^\alpha \equiv \int_1^\infty dy \frac{\mathrm{Re}\sum_\pm \pm[(y_1^\pm - y)(y - y_2^\pm) + i0^+]^\alpha}{(4\mu)^\sigma (y^2-1)^{1/2-\sigma}}, \tag{B9}$$

with $y_{1,2}^\sigma \equiv \sigma\mu \mp \sqrt{\mu^2 + 1 + 4\varepsilon\mu}$, $\sigma = \pm$ where the index 1 (2) belongs to the negative (positive) root.

APPENDIX C: LOGARITHMIC SINGULARITIES IN $\nu'(\varepsilon)$

In the superradiant regime ($\mu > 1$) we first consider $g^2\mu < 1$ near the ESQPT, writing the scaled energy $\varepsilon = -\frac{1}{2} + \delta$ with small δ. Expanding $y\pm$ and $z_\pm$ [Eq. (41)] in δ, one finds for the arguments of the elliptic integral in Eq. (43)

$$\frac{(y_+ - z_+)(y_- - z_-)}{(y_+ - y_-)(z_+ - z_-)} = 1 + r\delta + O(\delta^2), \quad \delta > 0 \tag{C1}$$

$$\frac{(y_+ - y_-)(z_+ - z_-)}{(y_+ - z_+)(y_- - z_-)} = 1 - r\delta + O(\delta^2), \quad \delta < 0, \tag{C2}$$

with the parameter

$$r \equiv \frac{2\mu^2 - g^2\mu(1+\mu)}{2(\mu-1)^2(g^2\mu - 1)}, \tag{C3}$$

and we use $K(1-|x|) = -\frac{1}{2}\ln\frac{|x|}{16} + O(x)$ to arrive at Eq. (45).

At $g^2\mu > 1$, the logarithmic singularity moves to the energy $\varepsilon = \varepsilon_g$ [Eq. (38)], where $z_\pm = g^2\mu$ and thus

$$\frac{(y_+ - z_+)(z_- - y_-)}{(y_+ - z_-)(z_+ - y_-)} \to 1. \tag{C4}$$

The value unity in the argument of the elliptic integral K again denotes the appearance of a logarithmic singularity. Finally, we numerically checked that the argument of K

$$\frac{(y_+ - y_-)^2 - (p_+ - p_-)^2}{4p_+p_-} = \theta(g^2\mu - 1), \quad \varepsilon = \varepsilon_g, \tag{C5}$$

which confirms that also for energies just below ε_g, we have a logarithmic divergence for $g^2\mu > 1$.

APPENDIX D: BOGOLIUBOV TRANSFORMATION (NORMAL PHASE)

To extract the collective excitation energies $\epsilon_\pm$ in the normal phase, we use the Holstein-Primakoff representation with a bosonic mode created by $b^\dagger$ [9,10],

$$J_+ = b^\dagger\sqrt{N - b^\dagger b}, \quad J_z = b^\dagger b - \frac{N}{2}, \tag{D1}$$

and expand the Hamiltonian (1) for large N, which leads us to

$$\mathcal{H} = \hbar\omega a^\dagger a + \hbar\omega_0 b^\dagger b + \hbar(\lambda_+ ab^\dagger + \lambda_- ab + \mathrm{H.c.}), \tag{D2}$$

where we defined $\lambda_\pm \equiv \lambda\frac{1\pm g}{2}$ and omitted a constant. We write $\mathcal{H}$ in canonical form [52] $\mathcal{H}/\hbar = \mathbf{a}^\dagger\alpha\mathbf{a} + \frac{1}{2}\mathbf{a}^\dagger\gamma\tilde{\mathbf{a}}^\dagger + \frac{1}{2}\tilde{\mathbf{a}}\gamma^\dagger\mathbf{a} = \frac{1}{2}\Lambda N\Sigma\tilde{\Lambda} - \frac{1}{2}\mathrm{Tr}\alpha$, with vectors $\mathbf{a}^\dagger \equiv (a^\dagger, b^\dagger)$, $\tilde{\mathbf{a}} \equiv (a, b)$, and $\Lambda \equiv (\mathbf{a}^\dagger, \tilde{\mathbf{a}})$, where the tilde converts rows into columns and vice versa. Here we used the canonical commutation relations, written in dyadic form with the 4×4 symplectic unity Σ as

$$[\tilde{\Lambda}, \Lambda] = \Sigma^{-1} = \begin{pmatrix} 0 & -1 \\ 1 & 0 \end{pmatrix}, \tag{D3}$$

and we defined the matrices

$$N \equiv \begin{pmatrix} \alpha & -\gamma \\ \gamma^\dagger & -\alpha \end{pmatrix}, \quad \alpha \equiv \begin{pmatrix} \omega & \lambda_+ \\ \lambda_+ & \omega_0 \end{pmatrix}, \quad \gamma \equiv \begin{pmatrix} 0 & \lambda_- \\ \lambda_- & 0 \end{pmatrix}. \tag{D4}$$

As in classical mechanics, a canonical transformation $\Lambda' = \Lambda M$ leaves Eq. (D3) invariant if $\tilde{M}\Sigma^{-1}M = \Sigma^{-1}$, i.e., if M is symplectic. The eigenvalues of $\mathcal{H}$ follow from the eigenvalues of N, which come in pairs $\pm\epsilon_\pm$. The product $\epsilon_+\epsilon_-$ thus simply follows from the determinant of N,

$$\begin{aligned} \det N &= (\epsilon_+\epsilon_-/\hbar^2)^2 = \lambda^4(1-\mu^{-1})(g^2 - \mu^{-1}) \\ &= (\omega\omega_0)^2(\mu-1)(g^2\mu - 1), \end{aligned} \tag{D5}$$

where in the last step we used $\mu = \lambda^2/\omega\omega_0$ [Eq. (2)], which confirms Eq. (47).

[1] K. Baumann, C. Guerlin, F. Brennecke, and T. Esslinger, Nature (London) **464**, 1301 (2010); K. Baumann, R. Mottl, F. Brennecke, and T. Esslinger, Phys. Rev. Lett. **107**, 140402 (2011).

[2] R. H. Dicke, Phys. Rev. **93**, 99 (1954).

[3] K. Hepp and E. Lieb, Ann. Phys. (NY) **76**, 360 (1973).

[4] F. Dimer, B. Estienne, A. S. Parkins, and H. J. Carmichael, Phys. Rev. A **75**, 013804 (2007).

[5] D. Nagy, G. Kónya, G. Szirmai, and P. Domokos, Phys. Rev. Lett. **104**, 130401 (2010).

[6] F. Piazza, P. Strack, and W. Zwerger, arXiv:1305.2928.

[7] M. J. Bhaseen, J. Mayoh, B. D. Simons, and J. Keeling, Phys. Rev. A **85**, 013817 (2012).

[8] H. Ritsch, P. Domokos, F. Brennecke, and T. Esslinger, Rev. Mod. Phys. **85**, 553 (2013).

[9] C. Emary and T. Brandes, Phys. Rev. Lett. **90**, 044101 (2003); Phys. Rev. E **67**, 066203, (2003).

[10] T. Brandes, Phys. Rep. **408**, 315 (2005).

[11] A. Altland and F. Haake, Phys. Rev. Lett. **108**, 073601 (2012).

[12] A. Altland and F. Haake, New J. Phys. **14**, 073011 (2012).

[13] M. Hayn, C. Emary, and T. Brandes, Phys. Rev. A **84**, 053856 (2011); **86**, 063822 (2012).

[14] A. Baksic, P. Nataf, and C. Ciuti, Phys. Rev. A **87**, 023813 (2013).

[15] P. Nataf and C. Ciuti, Phys. Rev. Lett. **104**, 023601 (2010); Nat. Commun. **1**, 72 (2010); Phys. Rev. Lett. **107**, 190402 (2011).

[16] L. Chirolli, M. Polini, V. Giovannetti, and A. H. MacDonald, Phys. Rev. Lett. **109**, 267404 (2012).

[17] D. Hagenmüller, S. De Liberato, and C. Ciuti, Phys. Rev. B **81**, 235303 (2010); G. Scalari, C. Maissen, D. Turčinková, D. Hagenmüller, S. De Liberato, C. Ciuti, C. Reichl, D. Schuh, W. Wegscheider, M. Beck, and J. Faist, Science **335**, 1323 (2012).

[18] P. Pérez-Fernández, P. Cejnar, J. M. Arias, J. Dukelsky, J. E. García-Ramos, and A. Relaño, Phys. Rev. A **83**, 033802 (2011).

[19] P. Pérez-Fernández, A. Relaño, J. M. Arias, P. Cejnar, J. Dukelsky, and J. E. García-Ramos, Phys. Rev. E **83**, 046208 (2011).

[20] R. Puebla, A. Relaño, and J. Retamosa, Phys. Rev. A **87**, 023819 (2013).

[21] P. Cejnar, M. Macek, S. Heinze, J. Jolie, and J. Dobeš, J. Phys. A: Math. Gen. **39**, L515 (2006).

[22] M. A. Caprio, P. Cejnar, and F. Iachello, Ann. Phys. (NY) **323**, 1106 (2008).

[23] P. Pérez-Fernández, A. Relaño, J. M. Arias, J. Dukelsky, and J. E. García-Ramos, Phys. Rev. A **80**, 032111 (2009).

[24] P. Ribeiro, J. Vidal, and R. Mosseri, Phys. Rev. Lett. **99**, 050402 (2007).

[25] P. Ribeiro, J. Vidal, and R. Mosseri, Phys. Rev. E **78**, 021106 (2008).

[26] F. T. Hioe, Phys. Rev. A **8**, 1440 (1973).

[27] M. A. Alcalde, A. L. L. de Lemos, and N. F. Svaiter, J. Phys. A **40**, 11961 (2007).

[28] M. Tavis and F. W. Cummings, Phys. Rev. **170**, 379 (1968); **188**, 692 (1969).

[29] Y. K. Wang and F. T. Hioe, Phys. Rev. A **7**, 831 (1973).

[30] K. Hepp and E. Lieb, Phys. Rev. A **8**, 2517 (1973).

[31] Our choice of coupling λ thus corresponds to half the coupling used in Ref. [9].

[32] By shifting integration variables, we have $\mathcal{Z}(\beta) = e^{-\beta E_0}\int_0^\infty dE e^{-\beta E}\tilde{\nu}(E)$ and thus $\nu(E) \equiv \tilde{\nu}(E - E_0) = \mathcal{L}^{-1}[\mathcal{Z}(\beta)e^{\beta E_0}e^{-\beta E_0}](E) = \mathcal{L}^{-1}[\mathcal{Z}(\beta)](E)$, where $\mathcal{L}^{-1}[\cdots]$ denotes the inverse Laplace transformation. Here it is understood that $\nu(E)$ vanishes below E_0. One obtains the value of E_0 (which is known for $\mathcal{H}$ [Eq. (1)] anyway) from an analysis of $\mathcal{Z}(\beta)$ for $\beta \to \infty$ (not discussed here).

[33] Note that this has to be contrasted with the usual calculations for the Dicke phase transition at finite temperature T [29,53], where the trace always runs over all the 2^N configurations of the pseudo-spin-$\frac{1}{2}$ states.

[34] M. A. Alcalde, M. Bucher, C. Emary, and T. Brandes, Phys. Rev. E **86**, 012101 (2012).

[35] C. M. Bender and S. A. Orszag, *Advanced Mathematical Methods for Scientists and Engineers* (McGraw-Hill, Singapore, 1978).

[36] Equation (31) is an example of the relation $\frac{\partial x}{\partial y}|_z \frac{\partial y}{\partial z}|_x \frac{\partial z}{\partial x}|_y = -1$ often used in thermodynamics if we write it in the form $\frac{\partial \nu}{\partial E}|_{\omega_0} \frac{\partial E}{\partial \omega_0}|_\nu \frac{\partial \omega_0}{\partial \nu}|_E = -1$ and take $E = E_0$, the ground-state energy.

[37] Fits with $\langle J_z\rangle(\varepsilon)/N = -0.12 + 0.12|\varepsilon + 0.5|^{1.5}$ for $\varepsilon > -0.5$ and $\langle J_z\rangle(\varepsilon)/N = -0.12 + 0.05|\varepsilon + 0.5|^{0.25}$ for $\varepsilon < -0.5$ [19] with parameters tuned visually work quite well within the band.

[38] O. Castaños, E. Nahmad-Achar, R. López-Peña, and J. G. Hirsch, Phys. Rev. A **83**, 051601 (2011).

[39] I. S. Gradshteyn and I. M. Ryzhik, *Table of Integrals, Series, and Products*, 5th ed. (Academic, New York, 1994).

[40] J. Vidal, S. Dusuel, and T. Barthel, J. Stat. Mech. (2007) P01015.

[41] D. M. Brink and G. R. Satchler, *Angular Momentum* (Oxford University Press, Oxford, 1962).

[42] There is also an improved semiclassical approximation derived by P. A. Braun, P. Gerwinski, F. Haake, and H. Schomerus [Z. Phys. B **100**, 115 (1996)] including an additional $\cos^2$ term with a classical action S_0 in the argument. This form (which is far too complicated for our purposes here) can, however, be reduced to the Brink-Satchler form (54) by taking the angular average over the $\cos^2$ term.

[43] We did not explicitly calculate $\langle J_z\rangle$ via the Hellmann-Feynman theorem (29), which is, in contrast to the Dicke case, cumbersome for the restricted Tavis-Cummings model.

[44] N. S. Tonchev, J. G. Brankov, and V. A. Zagrebnov, J. Optoelectron. Adv. Mater. **11**, 1142 (2009).

[45] It it not clear, though, what such an equivalence would mean in practical terms when calculating certain quantities in either of the two models.

[46] J. Vidal and S. Dusuel, Europhys. Lett. **74**, 817 (2006); G. Liberti, F. Plastina, and F. Piperno, Phys. Rev. A **74**, 022324 (2006); G. Liberti, F. Piperno, and F. Plastina, *ibid.* **81**, 013818 (2010).

[47] J. Wilms, J. Vidal, F. Verstraete, and S. Dusuel, J. Stat. Mech. (2012) P01023.

[48] R. Puebla and A. Relaño, arXiv:1305.3077v1.

[49] R. Kanamoto, L. D. Carr, and M. Ueda, Phys. Rev. A **81**, 023625 (2010).

[50] T. A. Zaleski, J. Phys. B **45**, 145303 (2012).

[51] T. Zibold, E. Nicklas, C. Gross, and M. K. Oberthaler, Phys. Rev. Lett. **105**, 204101 (2010).

[52] L. Huaixin and Z. Yongde, Int. J. Theor. Phys. **39**, 447 (2000).

[53] H. J. Carmichael, C. W. Gardiner, and D. F. Walls, Phys. Lett. A **46**, 47 (1973).